HAL
open science

Suffusion tests on cohesionless granular matter

Yacine Sail, Didier Marot, Luc Sibille, Alain Alexis

To cite this version:

Yacine Sail, Didier Marot, Luc Sibille, Alain Alexis. Suffusion tests on cohesionless granular matter. European Journal of Environmental and Civil Engineering, 2011, 15 (5), pp.799-817. 10.1080/19648189.2011.9693366 . hal-01007350

HAL Id: hal-01007350

https://hal.science/hal-01007350v1

Submitted on 10 Mar 2018

HAL is a multi-disciplinary open access archive for the deposit and dissemination of scientific research documents, whether they are published or not. The documents may come from teaching and research institutions in France or abroad, or from public or private research centers.

L'archive ouverte pluridisciplinaire **HAL**, est destinée au dépôt et à la diffusion de documents scientifiques de niveau recherche, publiés ou non, émanant des établissements d'enseignement et de recherche français ou étrangers, des laboratoires publics ou privés.

Suffusion tests on cohesionless granular matter

Experimental study

Yacine Sail — Didier Marot — Luc Sibille — Alain Alexis

Institut de Recherche en Génie Civil et Mécanique
Université de Nantes/CNRS
IUT de Saint-Nazaire, 58, rue Michel-Ange, F-44606 Saint-Nazaire cedex
didier.marot@univ-nantes.fr

ABSTRACT. *Under internal flow, hydraulic earth structures (dikes, levees, or dams) can incur a migration of particles possibly inducing a modification of hydraulic and mechanic characteristics. With the objective to characterize this phenomenon named internal erosion and its consequences on mechanical behaviour of granular materials, a large oedo-permeameter device has been developed. An axial load is applied on specimen together with a downward flow with a constant hydraulic gradient. During the testing time, the bench can measure the spatial change of density and interstitial pressure along the specimen. Axial deformation, injected flow and extracted mass are also measured during the testing time. Erosion of fine particles is characterised by an extraction (out of specimen) of these particles on downstream specimen part and also by a fine particles migration in the whole specimen. This suffusion induces a settlement and a localized increase of interstitial pressure. Afterwards a localized blowout appears and triggers large specimen deformations.*

RÉSUMÉ. *Sous l'action d'un écoulement interne, les ouvrages hydrauliques en terre (digues, levées, barrages) peuvent subir une migration de certaines particules, ce qui peut induire une modification des caractéristiques hydrauliques et mécaniques. Avec l'objectif de caractériser ce phénomène nommé érosion interne ainsi que ses conséquences sur le comportement mécanique de matériaux granulaires, un oedo-perméamètre de grandes dimensions a été développé. Une charge axiale est appliquée sur l'échantillon ainsi qu'un écoulement descendant sous gradient hydraulique constant. Au cours de l'essai, le banc expérimental permet la mesure de la variation spatiale de la densité et de la pression interstitielle le long de l'échantillon. La déformation axiale, le débit d'eau injecté et la masse extraite sont également mesurés au cours du temps. L'érosion de particules fines se caractérise par une extraction de ces particules dans la partie aval de l'échantillon et également par une migration de particules fines dans l'ensemble de l'échantillon. Cette suffusion entraîne un tassement et un accroissement local de la pression interstitielle. Ensuite un débourrage localisé se produit et déclenche de grandes déformations de l'échantillon.*

KEYWORDS: *soil erosion, suffusion, blowout, cohesionless soils, water flow, strain.*

MOTS-CLÉS : *érosion, suffusion, débourrage, sols non cohésifs, écoulement, déformation.*

1. Introduction

Seepage flow within earth structure (such as dam, dike or levee) can induce a detachment and a transport of fine particles from the structure or from its foundation. These phenomenons are named internal erosion processes and involve many parameters, some of them being coupled.

Initiation of internal erosion processes are influenced by geometric conditions such as grain size distribution (Kenney and Lau, 1985), porosity of soil and grain shape (Li, 2008) and by loading conditions as effective stress (Li, 2008) and hydraulic gradient (Skempton and Brogan, 1994). Depending on the process of internal erosion, confinement stress has a complex effect on internal erosion development (Bendahmane *et al*., 2008).

Internal erosion processes can modify hydraulic properties of soil as permeability but they can also modify mechanical behaviour of soil (Scholtès *et al*., 2010). Finally these modifications can induce instability of the earth structure. The occurrence of failures in new earth structures demonstrates the need of improving the knowledge of these phenomena and its consequences on mechanical behaviour of soil.

In uncracked soils, Fell and Fry (2007) distinguished two main phenomena of internal erosion: suffusion and backward erosion. Suffusion is the detachment and transport process of only fine particles whereas backward erosion concerns all grains.

Moffat and Fannin (2006) performed suffusion tests on gap graded specimens. They observed that suffusion process can lead to a localized failure and they defined the onset of this failure by the fast decrease in local hydraulic gradient at the upstream boundary of the specimen. This failure progressed rapidly in downward direction as a pipe in which the finer fraction was lost.

A new experimental bench was developed in order to study the hydromechanical behaviour of the soil before the onset of this failure. This device is described and tests are performed for specimens composed of a gap gradation of glass beads. Hydraulic and mechanical responses of specimens, submitted to an increasing hydraulic gradient are presented and analysed.

2. Erosion device

2.1. *Principle of the oedo-permeameter*

The main bench characteristics are summarized in Figure 1. Device is configured to enable specimen preparation which is saturated and consolidated under oedometric conditions. Specimen is subjected to seepage flow under a hydraulic gradient increasing by stages.

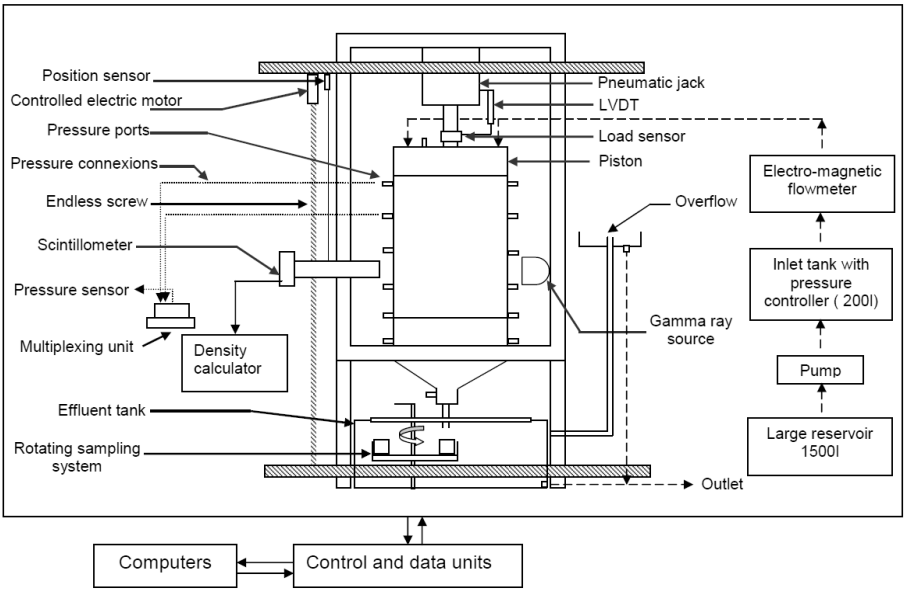

Figure 1. *Principle of the eodo-permeameter*

The bench (Marot *et al*., 2010) is composed of an oedo-permeameter cell with a funnel-shaped draining system which is connected to a collecting system. The bench comprises also an axial loading system, a hydraulic control system and a gammadensitometric system. The control and acquisition part is provided by two units connected to two computers. All these components are detailed below.

2.2. *Oedo-permeameter cell and collecting system*

With the aim to observe specimen during testing time, the rigid wall cell is made of a Plexiglas tube. Internal cell diameter is $\Phi_{cell} = 280$ mm and the specimen height can reach 600 mm. It is worth noting that the oedo-permeameter cell allows to test specimen with a maximum grain size $D_{max} = 9$ mm (equivalent to a cell factor $D_{max}/\Phi_{cell} = 30$) and a slenderness ratio of 2. The two ends of Plexiglas tube are reinforced by stainless steel plates. Cell wall is equipped with twelve pressure ports (two arrays of six pressure ports, with a vertical spacing of 100 mm, face to face on opposite cell sides), a pressure port is placed on piston base plate (*i.e.* at the specimen-piston interface) and a fourteenth port is located below the specimen on the draining system. In order to avoid discrepancy between two pressure transducers, pressure ports are connected to a multiplex unit which is connected to a single pressure sensor (Alexis *et al*., 2004).

Thanks to several specimen supports, specimen with different heights can be tested. A stainless steel mesh screen is placed on specimen support. This 15 mm thick mesh screen has a 10 mm pore opening size in order to allow the migration of all grains. With a rim, different wire meshes can be fixed on the mesh screen in order to take into account the effect of pore opening size on internal erosion (Marot *et al*., 2009). To eliminate any particle migration between mesh screen and cell, a geotextile is placed between wire screen edge and rigid wall of cell.

The top plate of the cell has two inlet ports (10 mm in diameter each, and connected to an upstream gate) and the cell base has a vertical funnel-shaped draining system, specially designed to avoid clogging. The opening of draining system is controlled by a pneumatic gate at the bottom of the vertical funnel. Outlet pipe is in glass in order to permit the measurement of effluent transparency by means of an optical sensor (Bendahmane *et al*., 2008).

The collecting system is composed of an effluent tank which has an overflow outlet with a 0.08 mm mesh in order to catch the extracted fine particles. Effluent tank is equipped with a rotating sampling system containing several beakers for the effluent sampling.

2.3. *Axial loading system*

A piston, a pneumatic cylinder and a reaction frame compose the axial loading system. The piston comprises two perforated plates which are made of 15 mm thick stainless steel. A 61 mm thick layer of gravel separates the two plates in order to diffuse the injected fluid uniformly at the top of the specimen. Two gaskets are bonded to the piston edge to avoid any parasitic particle displacements between piston and cell wall.

Axial effective stress on the top of specimen is generated by a pneumatic cylinder which has a 200 mm translation range in order to maintain the axial stress even in the case of great specimen settlements. A load cell measures the axial force on the loading rod. The piston displacements and thus the specimen settlements are measured by a Linear Variable Differential transducer (LVDT).

The pneumatic cylinder is mounted on a framework. This framework supports also the oedo-permeameter cell which is mounted on a large ball bearing for the axial cell rotation.

2.4. *Hydraulic control system*

Hydraulic system is composed of two reservoirs and a pump. A 1 500 litre storage reservoir is supplied by public water system and placed in a temperature-controlled chamber.

This reservoir supplies with a pump a 200 L tank equipped with an air pressure controller. The water head applied on the specimen top face is measured thanks to a pressure transducer connected to the pressure port on the piston base. The seepage flow is measured with two electromagnetic flowmeters (of different capacities 120 L/min and 480 L/min) located between the pressure tank and the oedo-permeameter cell.

2.5. *Gammadensitometric system*

The gammadensitometric bench was developed by Alexis *et al.* (2004). It comprises a radioactive gamma-ray source and a scintillation counter on the opposite cell side. These components are bonded on a carriage moving in vertical direction thanks to an endless screw and a controlled electric motor. The position of the carriage is measured by a position transducer. According to a previous gauging data, a density calculator counts the scintillometer impulses and calculates the mean density of the part of specimen located 25 mm around the scintillation counter focal axis.

2.6. *Monitoring and data acquisition system*

Device control and data acquisition is provided by two data units. The master controls the gammadensitometric bench motor and the multiplex pressure transducer. It is also in charge of acquisition of: specimen density, carriage position and water head at all pressure ports. Two travelling velocities are used for the gammadensitometric carriage, a cruising speed and an approach speed to limit both travelling duration and position discrepancy. This master unit drives the run of the slave data acquisition unit.

The slave unit carries out the measurements from the load sensor, the settlement sensor and seepage flowmeters.

3. Specimen properties and test procedure

The tested material is a mixture of glass beads. This cohesionless material allows to compare our results with experimental campaign performed by Moffat and Fannin (2006) with a large permeameter.

3.1. *Material properties*

Figure 2 plots the grain size distribution of tested glass mixture (named G4-C by Moffat and Fannin, 2006) and the grain size distributions of the coarse fraction C and fine fraction F.

According to Moffat and Fannin (2006), the fine fraction F is equivalent to a fine sand with a coefficient of uniformity $C_u = 1.4$ and $d_{85} = 0.19$ mm (where d_{85} is the sieve size for which 85% of the soil mass is finer). Fraction C is equivalent to coarse sand with $C_u = 1.7$ and $d_{10} = 1.4$ mm. G4-C grading is composed of 40% by weight of F and 60% of C and it is characterized by a gap. The mixture is prepared by mixing coarse and fine fraction during 3 minutes with 10% water content in a mixing machine. Afterwards, homogeneity is verified by size distribution measurements.

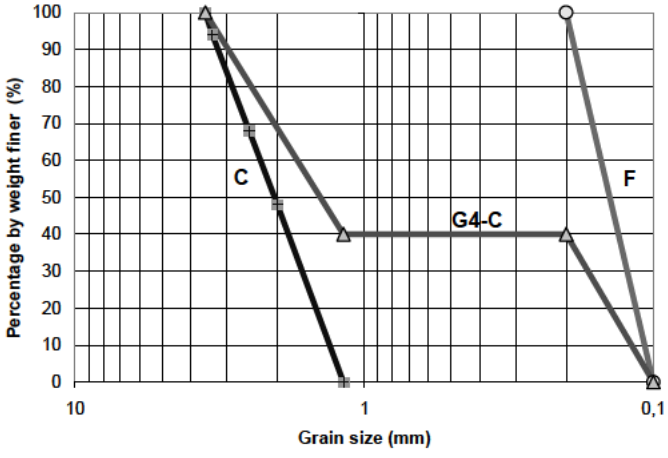

Figure 2. *Grain size distribution of glass beads*

3.2. *Test procedure*

A wire mesh with a 1.25 mm pore opening size is fixed on wire mesh screen in order to allow only the migration of fine particles.

First the cell is filled with water to saturate by gravity flow the pressure connexions, the multiplex unit and the pressure sensor.

In conformity with specimen creation technique used by Moffat and Fannin (2006), specimen is prepared in several layers by slurry deposition. The total dry mass of glass beads constituting the specimen is 51.03 kg and the initial specimen height is 45 cm. A wire mesh of 0.08 mm is placed on specimen top face to avoid fine particles migration into the piston.

Specimen is consolidated under a 25 kPa axial loading and with double drainage conditions (dissipation of excess interstitial pressure in upward and downward directions).

At the end of specimen preparation, a loss of fine particles is measured which represents around 2.1% of total fine mass. The profile of density measurement (cf. Figure 3) shows a density which varies from 2.07 g/cm^3 to 2.12 g/cm^3.

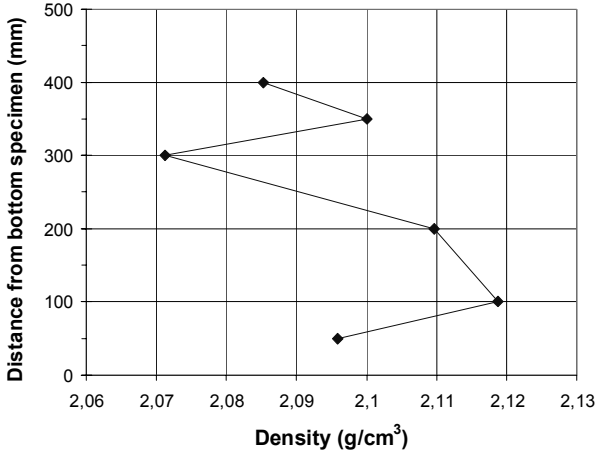

Figure 3. *Initial profile of density*

Comparison of the initial dry mass of beads composing the specimen and density measurements of each specimen layer is used to estimate the saturation ratio S_r of the specimen. Initial saturation ratio is equal to 96% and this high value advocates the procedure used to prepare the specimen.

Data acquisition is started afterwards specimen is subjected to a downward seepage flow. Data are recorded with a periodicity of 1 second and the effluent sampling is performed within a 6 minute period.

In conformity with procedure used by Moffat and Fannin (2006), multi-stage flow was increased from an initial value of global hydraulic gradient equal to unity and with an increment about unity. Each stage of global hydraulic gradient was one hour duration.

For this specimen height, Figure 4 shows positions of used pressure ports (numbered H6, L1 to L5 and R1 to R5) and heights of density measurement stations (section S1 to section S6) with respect to specimen bottom face.

At the end of each hydraulic gradient stage, the specimen is isolated by simultaneous closing of upstream and downstream gates and the controlled pressure tank is filled.

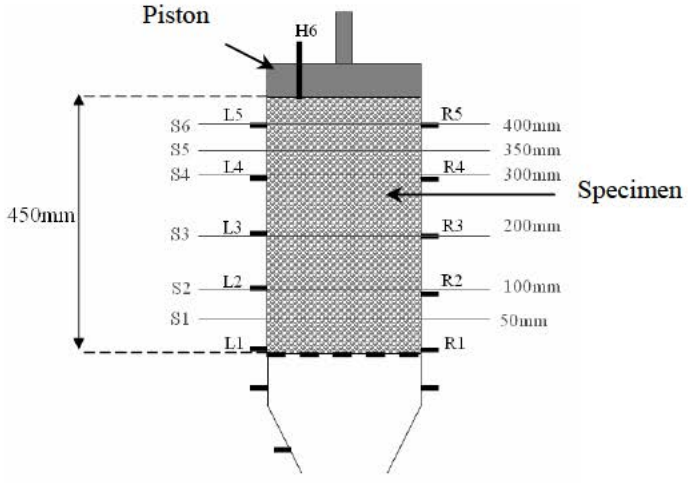

Figure 4. *Position of interstitial pore pressure ports and stations of density measurement*

4. Test results

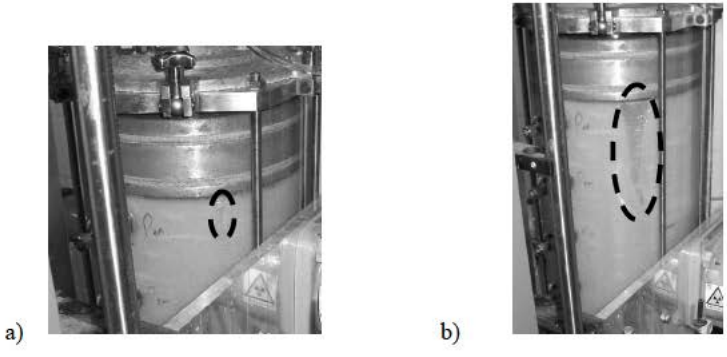

Figure 5. *a) initiation of localized blowout (global hydraulic gradient $i_5 = 4.9$, $t = 310$ min); b) downward progression of localized blowout ($t = 312$ min)*

Five stages of hydraulic gradient were applied on the specimen, with successive average values: $i_1 = 1$, $i_2 = 2$, $i_3 = 3$, $i_4 = 4$ and $i_5 = 4.9$. The duration of each stage was 60 min for the four first stages and a strong localized blowout occurred 52 min after the beginning of the fifth stage (corresponding to a total duration $t = 312$ min). This blowout results to the forming of a zone in which the finest fraction seems to be totally lost and initially observed at the specimen top interface (see Figure 5a). This

localized blowout progressed in downward direction (see Figure 5b) close to the positions of pressure ports R5, R4, R3, R2 and finally R1.

Figure 6 plots the instantaneous values of seepage flow and applied hydraulic gradient for the five stages. During the first hydraulic gradient stage ($i_1 = 1$), the seepage flow was 0.5 L/min and for the three following stages its value was 0.8 L/min, 1.2 L/min, 1.5 L/min respectively. For the fifth stage ($i_5 = 4.9$), the flow was 2 L/min during 52 minutes and finally sharply increased to reach 6 L/min.

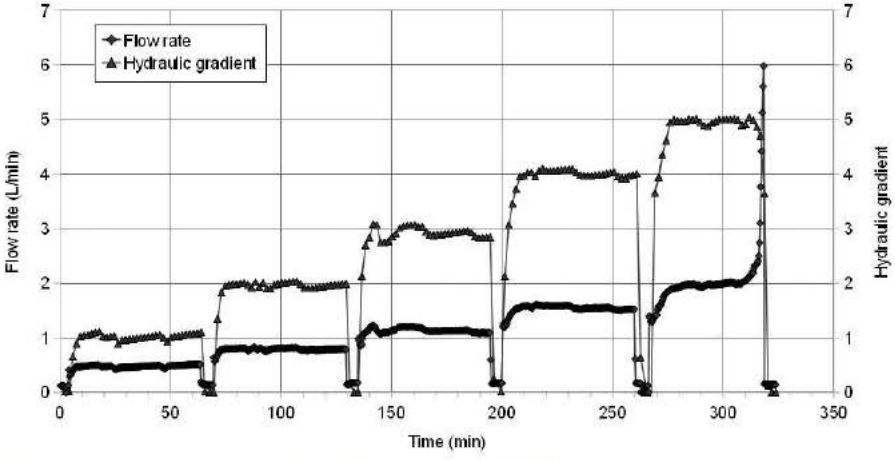

Figure 6. *Instantaneous values of flow rate and hydraulic gradient*

For the first stage, the specimen hydraulic conductivity was $k = 1.2\ 10^{-4}$m/s. For the stage 2 up to the beginning of stage 5, hydraulic conductivity was constant $k = 1.1\ 10^{-4}$m/s but then suddenly it increased up to $3.3\ 10^{-4}$m/s.

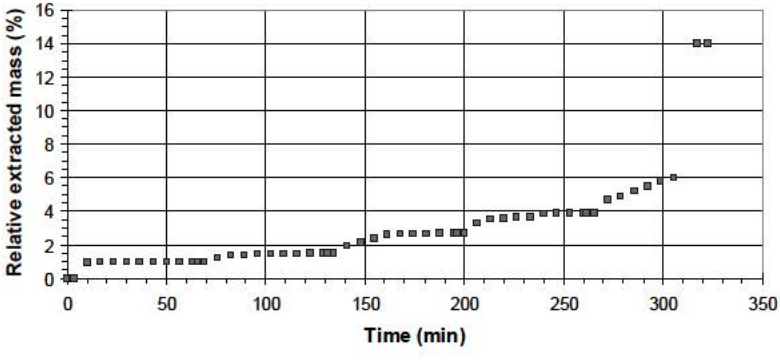

Figure 7. *Instantaneous values of relative extracted mass*

Figure 7 shows the evolution of relative extracted mass which is the ratio of cumulative mass of extracted fine particles to initial mass of fine particles in specimen. Application of the four first stages of hydraulic gradient induced a small extraction of fine particles. Each increment of applied hydraulic gradient induced an increase of relative extracted mass for about twenty minutes and then relative extracted mass stayed almost constant up to the end of stages.

At the end of all four first stages, relative extracted mass was successively: $m_{F\ extracted}/m_{F\ initial}$ = 1%, 1.5%, 2.7% and 3.9%. During the 50 first minutes of fifth stage, relative extracted mass increased by 2% to reach 6% at t = 306 min. The occurrence of strong blowout was accompanied by a great increase of relative extracted mass which reached 14% at t = 317 min.

Figure 8 shows the evolution of axial strain for the five stages. At the end of the first stage, axial strain was negligible and then it increased regularly. Axial strain was: ε_{axial} = 0.3%, 1%, and 1.6% for stages 2, 3 and 4 respectively. At the end of the fourth stage, axial strain did not totally stabilize announcing the strong specimen destabilization at stage 5. Application of the fifth stage induced an increase of axial strain of 2% (ε_{axial} = 3.8%, at t = 317 min) and finally strong blowout is correlated with a large axial strain (ε_{axial} = 4.9%, at t = 320 min).

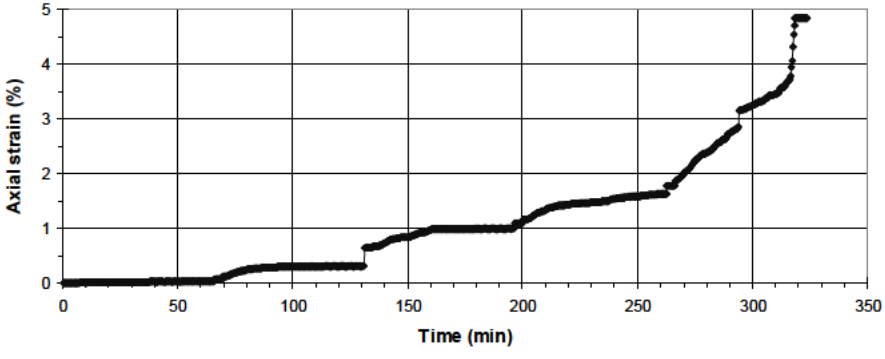

Figure 8. *Instantaneous values of axial strain*

The similar kinetics of increase for extracted mass and settlement can be noted along the whole test duration. Regardless the final phenomenon of blowout development, two hypotheses about the process can be considered:

– fine particle extraction at specimen bottom induces a migration of fine particles concerning the whole specimen and causing the settlement,

– fine particles extraction at specimen bottom induces an instability located on downstream part and causing a specimen translation without any migration of fine particle in the specimen centre part.

Figure 9 shows instantaneous values of relative density changes for each section (S1 to S6). Relative density is the ratio of instantaneous density changes to initial density. Two types of density variations were measured during test:

– decrease of density in the downstream part of specimen (sections S1, S2 and S3) with a final relative change of about -1.4%,

– increase of density in the upstream part (sections S4, S5 and S6) with a final relative change between +1.5% (for Section 4), +3.7% (for S5) and +5.1% (for S6).

It is worth noting that the localized blowout was developed outside of the measurement zone of gammadensitometer (see Figure 5b).

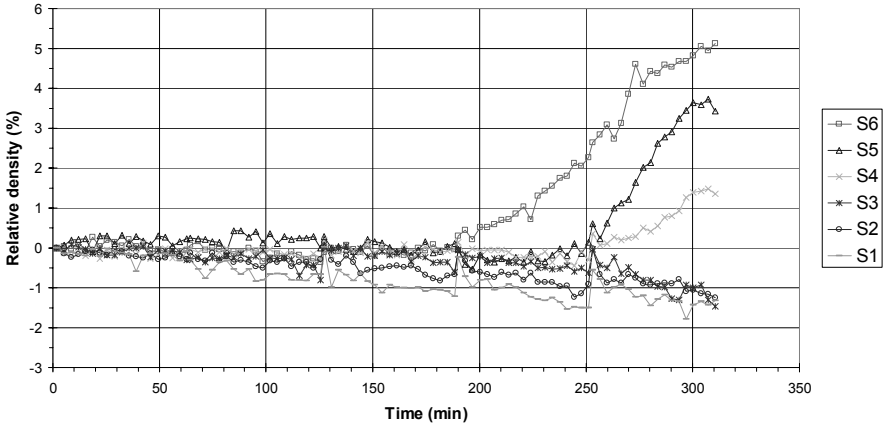

Figure 9. *Instantaneous values of relative density*

In specimen upstream part (section S4 to S6), and in particular for the upper section S6 where incoming fine particles is limited (or even nil), the increase of density could result from the compaction of the granular assembly. This compaction has been triggered by the loss of fine particles carried away by water flow, allowing the rearrangement of the other remaining particles under the vertical stress applied.

In specimen downstream part the density reduction can be explained by an important loss of fine particles not counterbalanced by fine particles arriving from the upstream part nor by a compaction of the coarse particle fraction.

Consequently, changes of density seem to show that erosion process concerns the whole specimen, especially during the four first stages of hydraulic loading.

5. Discussion

5.1. *Comparison of extracted mass with axial strain and density*

The objective of this comparison is to validate the measurements of density. Instantaneous value of density ρ_i for specimen layer i, can be expressed by:

$$\rho_i(t) = \frac{M_i(t)}{V_i(t)} = \frac{M_{w\,i}(t) + M_{s\,i}(t)}{V_i(t)} \qquad [1]$$

where $M_i(t)$ and $V_i(t)$ are respectively the global mass and the volume of the saturated specimen layer i at time t; $M_{w\,i}(t)$ and $M_{s\,i}(t)$: the mass of water and glass beads respectively in layer i at time t.

The mass of water and glass beads can be determined by:

$$M_{w\,i}(t) = \rho_w V_{w\,i}(t) = \rho_w S_r V_{v\,i}(t) = \rho_w S_r \left(V_i(t) - V_{s\,i}(t)\right) \qquad [2]$$

$$M_{s\,i}(t) = \rho_s \mathrm{V}_{s\,i}(t) \qquad [3]$$

where $V_{v\,i}(t)$ is the volume of void in layer i at time t; $V_{s\,i}(t)$: the volume of glass beads in layer i at time t; ρ_w and ρ_s: the density of water and glass beads respectively. The saturation ratio S_r is assumed constant during the test.

By combining Equations [1], [2] and [3] it comes:

$$\rho_i(t) = \frac{\rho_s V_{s\,i}(t) + \rho_w S_r \left(V_i(t) - V_{s\,i}(t)\right)}{V_i(t)} \qquad [4]$$

and the volume of glass beads in layer i can be expressed by:

$$V_{s\,i}(t) = \frac{V_i(t)\left(\rho_i(t) - \rho_w S_r\right)}{\rho_s - \rho_w S_r} \qquad [5]$$

Only the volume of the upper layer $V_6(t)$ changes with time:

$$V_6(t) = V_6 - S\,\Delta L(t) \qquad [6]$$

where V_6 is the initial volume of upper layer, S: the specimen cross section and $\Delta L(t)$: the instantaneous value of axial settlement.

Then the instantaneous value of specimen dry mass $M_d(t)$ can be calculated by:

$$M_d(t) = \rho_s \sum_{i=1}^{6} V_{s\,i}(t) \qquad [7]$$

These values of specimen dry mass calculated from measurements of settlement and density are compared with the difference of initial dry mass and measured values of extracted dry mass of beads collected at the outlet of the specimen (see Figure 10).

Contrary to the determination based on extracted dry mass measurements, specimen dry mass calculated from measurements of settlement and density doesn't take into account fine particle loss which occurs during specimen preparation. This difference contributes to explain the slight discrepancy between the two time series of specimen dry mass at the beginning of the test. As the blowout occurred outside of the measurement zone of gammadensitometer, specimen dry mass calculated from measurements of settlement and density is overestimated from the blowout creation time.

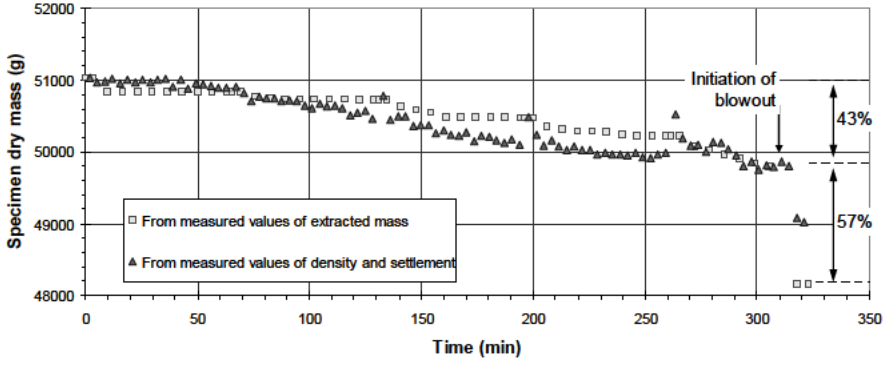

Figure 10. *Values of specimen dry mass determined by two methods versus time*

It can be noted that the decrease of dry specimen mass before the occurrence of blowout represents about 43% of the total decrease of specimen mass (see Figure 10).

The low discrepancy (less than 5%) between these two time series of specimen dry mass validates the measurements of density.

5.2. *Identification and characterization of erosion processes*

At the end of test, five bead samples were extracted in each specimen layer. One sample was realized in the localized blowout (profile A on Figure 11a), three other samples along the specimen-cell boundary (profiles B, C and D) and one in the centre (see Figure 11b).

a)

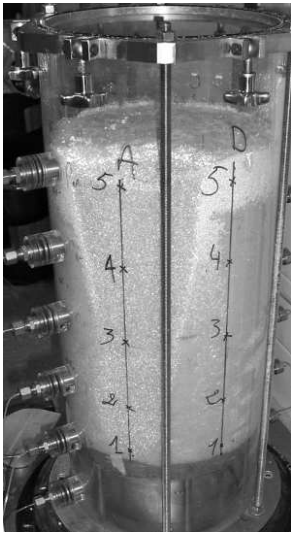

b)

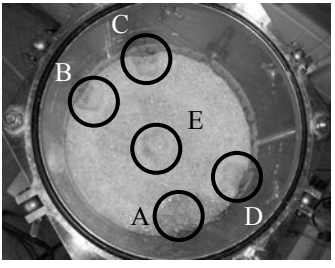

Figure 11. *Localization of sampling profiles a) side view, b) top view*

Figure 12 shows two profiles of fine mass percentage as a function of the distance from the specimen bottom. For each layer, one profile represents the fine percentage in localized blowout (profile A) and the second corresponds to the average value of fine percentage from the four other samples.

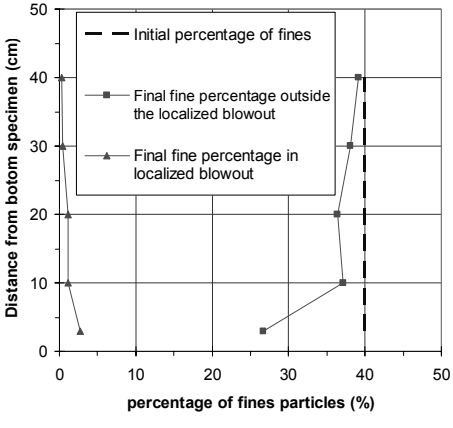

Figure 12. *Vertical profiles of fine percentage in specimen*

In localized blowout, percentage of fines increases in downward direction from 0.4% to 2.8%. This evolution shows a translation in downward direction of all fine particles in this zone. Outside of this localized blowout, the profile of fine percentage has an opposite evolution: from 39.2% in upper layer to 26.7% in the bottom layer. This downward decrease of fine percentage seems to characterize a regressive erosion of fine particles. With the exception of localized blowout, this process concerns the whole section and can be named suffusion. In addition, the low percentage of fine in the very bottom part can be partially due to the loss of fine particles during the specimen preparation.

With the objective to estimate the proportion of each erosion process in the total extracted bead mass, the volume of the localized blowout was estimated by image processing from pictures of upper cross section of each layer (see Figure 13).

For each picture is computed the area of the section of the localized blowout. This section is supposed constant in the concerned layer. Thus the volume of the blowout is determined by the product of blowout section by layer thickness. Thanks to the initial value of dry density and with the final percentage of fines in the blowout, it can be concluded that the extracted mass of fine particles in the blowout represents 56% of the total extracted mass. This mass percentage is in good agreement with the previous percentage determined with the measured values of extracted mass from the time of blowout creation and displayed in Figure 10.

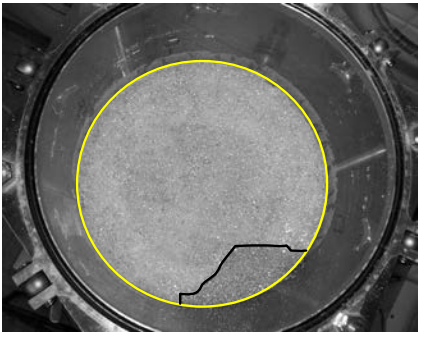

Figure 13. *Upper cross section of layer (Section 5)*

Although suffusion process was less perceptible than localized blowout, it represents a major contribution to the total extracted mass (about 43%, see Figure 10).

5.3. *Initiation of localized instability*

Moffat and Fannin (2006) speculate the onset of failure is governed by a great drop of local hydraulic gradient which appeared at $t = 920$ s during their test. With the assumption that the water pressure under the specimen stayed constant during time test, the authors reinterpret the variation of local hydraulic gradient measured by Moffat and Fannin (2006) in terms of local hydraulic head (see Figure 14).

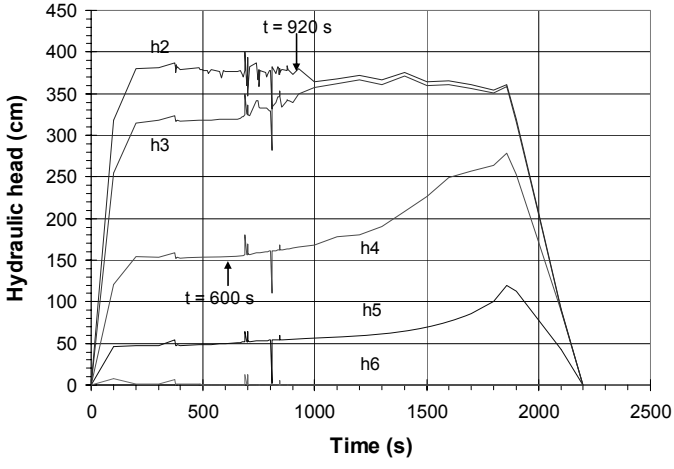

Figure 14. *Time series of hydraulic head (determined from test of Moffat and Fannin, 2006)*

It can be observed from $t = 600$ s, that hydraulic head in elevation 4 (which corresponds to the middle of specimen) increased slowly (indicated by an arrow on profile h4 in Figure 14). This increase preceded the drop of local hydraulic gradient (at $t = 920$ s).

During the four first stages of test described in this paper, spatial and time evolutions of local hydraulic head didn't evolve significantly.

Figure 15 represents profiles of hydraulic head during the fifth stage.

At $t = 5$ min hydraulic head decreased because of the downstream gate opening.

At $t = 47$ min, hydraulic head on pressure port R4 increased of about $\Delta h = 7$ cm (corresponding to an overpressure of 0.7 kPa). Two minutes later, a similar increase was detected on pressure port R3. These increases of interstitial pressure preceded the onset of localized blowout (at $t = 52$ min) which developed in downward direction close to the position of pressure ports R5 to R1.

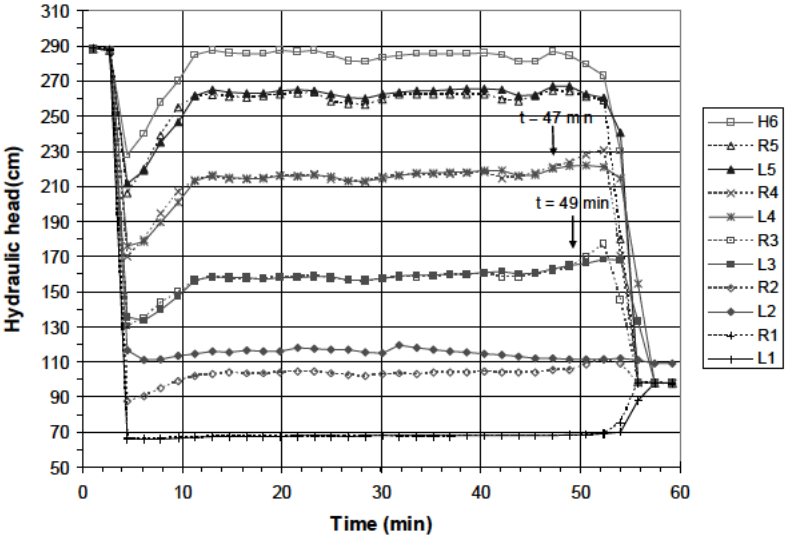

Figure 15. *Instantaneous values of hydraulic head (i_5 = 4.9)*

Another test was performed on the same type of gap graded specimen. Twenty minutes after the beginning of hydraulic gradient stage i = 4.8, a localized blowout developed exactly along the positions of pressure ports R5 to R1.

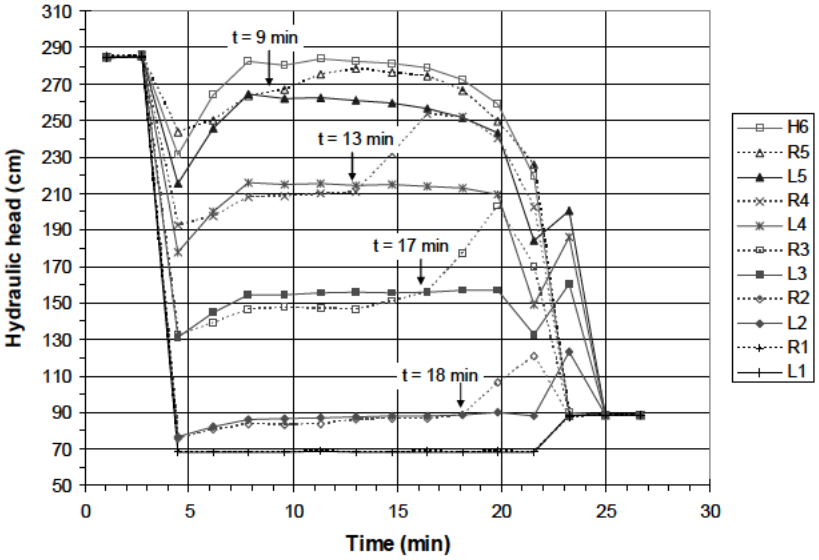

Figure 16. *Instantaneous values of hydraulic head, second test (i = 4.8)*

Figure 16 shows the profiles of hydraulic head measured during this second test. At $t = 9$ min, the hydraulic head on pressure port R5 slightly increased. Four minutes later, a fast increase of hydraulic head on pressure port R4 of about $\Delta h_{R4} = 42$ cm was detected.

At $t = 17$ min the hydraulic head on R3 increased about $\Delta h_{R3} = 47$ cm and one minute later on port R2: $\Delta h_{R2} = 32$ cm. This increase of interstitial pressure which appeared in the specimen top and progressed in downstream direction may be due to a filtration of a part of eroded particles. This filtration induced a clogging which generates an interstitial overpressure. During a few minutes, this interstitial overpressure increased and suddenly it triggered the onset of the localized blowout. Finally the drop of local hydraulic gradient appears as a consequence of the fast and large development of the blowout.

6. Conclusion

An experimental bench was designed to study initiation and development of suffusion and its consequences on the hydraulic and mechanical behaviour of cohesionless soils. The device and experimental procedure are detailed. Results of tests performed on gap graded glass beads specimen are reported. On the downstream specimen part, a loss of fine particles was detected and also an erosion of fine particles in the whole specimen. Two different processes of erosion were observed: suffusion and blowout. Suffusion is responsible of about 43% of the total extracted mass. Suffusion process is a diffused phenomenon and is accompanied by a filtration of some eroded particles. This filtration created a clogging which induced a localized interstitial overpressure and finally it led to a localized blowout. Finally the hydraulic conductivity has been multiplied by three and the axial deformation reaches 5%.

For this initial percentage of 40% of fine particles, axial strain and extracted mass had a similar kinetics of increase. Further studies are required to confirm this behaviour with varying particle fractions.

The experiment setup will be used on different types of soil, in order to improve our understanding of the internal erosion processes.

Acknowledgement

We wish to acknowledge the support of the French National Research Agency (project ANR-ERINOH) and the support of the French Institute for Applied Research and Experimentation in Civil Engineering (IREX). The authors wish to express their gratitude to R. Coué, D. Fournol and F. Gervot, Technicians at the University of Nantes, for their assistance in the assembly of the experimental bench.

7. References

Alexis A., Le Bras G., Thomas P., "Experimental bench for study of settling-consolidation soil formation", *Geotechnical Testing Journal*, vol. 27, n° 6, 2004, p. 557-567.

Bendahmane F., Marot D., Alexis A., "Parametric study of suffusion and backward erosion", *Journal of Geotechnical and Geoenvironmental Engineering (ASCE)*, vol. 134, n° 1, 2008, p. 57-67.

Fell R., Fry J.J., *Internal Erosion of Dams and their Foundations*, Editors, Taylor & Francis Publisher, 2007.

Kenney T.C., Lau D., "Internal stability of granular filters", *Canadian Geotechnical Journal*, vol. 22, n° 2, 1985, p. 215-225.

Li M., Seepage induced instability in widely graded soils. PhD Thesis, University of British Colombia, Vancouver, Canada, 2008

Marot D., Bendahmane F., Rosquoet F., Alexis A., "Internal flow effects on isotropic confined sand-clay mixtures", *Soil & Sediment Contamination, an Int. Journal*, vol. 18, n° 3, 2009, p. 557-567.

Marot D., Sail Y., Alexis A., "Experimental bench for study of internal erosion in cohesionless soils", *5th International Conference on Scour and Erosion (ISCE-5)*, San Francisco, USA, 7-10 November 2010, p. 418-427.

Moffat R., Fannin R.J., "A large permeameter for study of internal stability in cohesionless soils", *Geotechnical Testing Journal*, vol. 29, n° 4, 2006, p. 1-7.

Scholtès L., Hicher P.Y., Sibille L., "Multiscale approaches to describe mechanical responses induced by particle removal in granular materials", *Comptes rendus mécaniques*, vol. 338, n° 10-11, 2010, p. 627-638.

Skempton A.W., Brogan J.M., "Experiments on piping in sandy gravels", *Géotechnique*, vol. 44, n° 3, 1994, p. 449-460.